



This is a repository copy of *Highly variable latest Pleistocene-Holocene incremental slip rates on the Awatere fault at Saxton River, South Island, New Zealand, revealed by lidar mapping and luminescence dating.*

White Rose Research Online URL for this paper:

<https://eprints.whiterose.ac.uk/124358/>

Version: Published Version

Article:

Zinke, R. orcid.org/0000-0003-4174-3137, Dolan, J.F. orcid.org/0000-0002-6799-5781, Rhodes, E.J. orcid.org/0000-0002-0361-8637 et al. (2 more authors) (2017) Highly variable latest Pleistocene-Holocene incremental slip rates on the Awatere fault at Saxton River, South Island, New Zealand, revealed by lidar mapping and luminescence dating. *Geophysical Research Letters*, 44 (22). 11,301-11,310. ISSN 0094-8276

<https://doi.org/10.1002/2017GL075048>

Reuse

Items deposited in White Rose Research Online are protected by copyright, with all rights reserved unless indicated otherwise. They may be downloaded and/or printed for private study, or other acts as permitted by national copyright laws. The publisher or other rights holders may allow further reproduction and re-use of the full text version. This is indicated by the licence information on the White Rose Research Online record for the item.

Takedown

If you consider content in White Rose Research Online to be in breach of UK law, please notify us by emailing eprints@whiterose.ac.uk including the URL of the record and the reason for the withdrawal request.



eprints@whiterose.ac.uk
<https://eprints.whiterose.ac.uk/>



RESEARCH LETTER

10.1002/2017GL075048

Key Points:

- Incremental fault slip rates for the dextral Awatere fault were highly variable throughout latest-Pleistocene and Holocene time
- Extreme variations in slip rate suggest changes in fault strength and/or loading rate over time
- Care should be used when interpreting fault slip rates in the context of geodetic observations or probabilistic seismic hazard assessment

Supporting Information:

- Supporting Information S1

Correspondence to:

R. Zinke,
rzinke@usc.edu

Citation:

Zinke, R., Dolan, J. F., Rhodes, E. J., Van Dissen, R., & McGuire, C. P. (2017). Highly variable latest Pleistocene-Holocene incremental slip rates on the Awatere fault at Saxton River, South Island, New Zealand, revealed by lidar mapping and luminescence dating. *Geophysical Research Letters*, 44. <https://doi.org/10.1002/2017GL075048>

Received 25 JUL 2017

Accepted 29 SEP 2017

Accepted article online 9 OCT 2017

Highly Variable Latest Pleistocene-Holocene Incremental Slip Rates on the Awatere Fault at Saxton River, South Island, New Zealand, Revealed by Lidar Mapping and Luminescence Dating

Robert Zinke¹ , James F. Dolan¹ , Edward J. Rhodes² , Russ Van Dissen³ , and Christopher P. McGuire⁴ 

¹Department of Earth Sciences, University of Southern California, Los Angeles, CA, USA, ²Department of Geography, University of Sheffield, Western Bank, UK, ³GNS Science, Lower Hutt, New Zealand, ⁴Department of Earth, Planetary, and Space Sciences, University of California, Los Angeles, CA, USA

Abstract Geomorphic mapping using high-resolution lidar imagery and luminescence dating reveal highly variable incremental Holocene-latest Pleistocene slip rates at the well-known Saxton River site along the Awatere fault, a dextral strike-slip fault in the Marlborough Fault System, South Island, New Zealand. Using lidar and field observations, we measured seven fault offsets recorded by fluvial terraces and bedrock markers. Improved dating of the offsets is provided by post-IR-IRSL₂₂₅ luminescence ages. Incremental slip rates varied from <2 mm/yr to >15 mm/yr over intervals of thousands of years and tens of meters of slip, demonstrating order-of-magnitude temporal variations in rate at a single site. These observations have basic implications for earthquake fault behavior, lithospheric mechanics, discrepancies between geodetic and geologic slip rates, and probabilistic seismic hazard assessment.

1. Introduction

Fault slip rates reflect the interplay among multiple geologic and geodynamic processes that are as-yet not fully understood. Such understanding, however, is essential to developing theories of lithospheric mechanics and can inform debates such as those over the role of faults in accommodating relative plate motion (e.g., Tapponier & Molnar, 1976), and discrepancies between geodetically inferred slip deficit rates and geologic fault slip rates (e.g., Dolan et al., 2016). Moreover, fault slip rates provide a basic input for earthquake recurrence models used in probabilistic seismic hazard assessment (e.g., Field et al., 2014, 2015, 2017). Studies of fault behavior in a variety of tectonic settings are necessary to determine whether slip rates vary in predictable ways, and what factors influence their behavior. The key problem is that there exist far too few incremental fault slip rate records from faults and fault networks around the world to allow for full system-level analysis of the consistency of fault slip in time and space. The dearth of such data sets leads us to revisit the well-known Saxton River site on the Awatere fault in northern South Island, New Zealand. We use high-resolution lidar microtopographic data and a newly developed infrared stimulated luminescence (IRSL) dating protocol to determine incremental Holocene-latest Pleistocene slip rates for the Awatere fault at this site. Such incremental slip rate records are key to understanding fault behavior through time and space, with basic implications for earthquake recurrence, system-level fault interactions, and plate boundary mechanics.

2. The Saxton River Site

The Awatere fault is a principal right-lateral strike-slip fault within the Marlborough Fault System (MFS), a network of mainly right-lateral faults that accommodate strain between the dextral-reverse Alpine fault and the Hikurangi subduction margin (Figure 1) (e.g., Wallace et al., 2012). The Saxton River site consists of six progressively offset fluvial terraces and a bedrock spur (Figure 1). At the end of the Last Glacial Maximum, gravels aggraded throughout the Saxton River valley, carving the valley edges and filling the valley to the elevation of the highest (T1) terrace tread (Bull & Knuepfer, 1987; Mason et al., 2006). Throughout latest Pleistocene-Holocene time, the Saxton River has incised into the fill sequence, creating “degradational” terrace surfaces or “treads” (T2–T6) at progressively lower elevations where the river floodplain temporarily stabilized for periods of hundreds to thousands of years, depositing relatively thin units of sandy gravel and silts (Figures 1 and

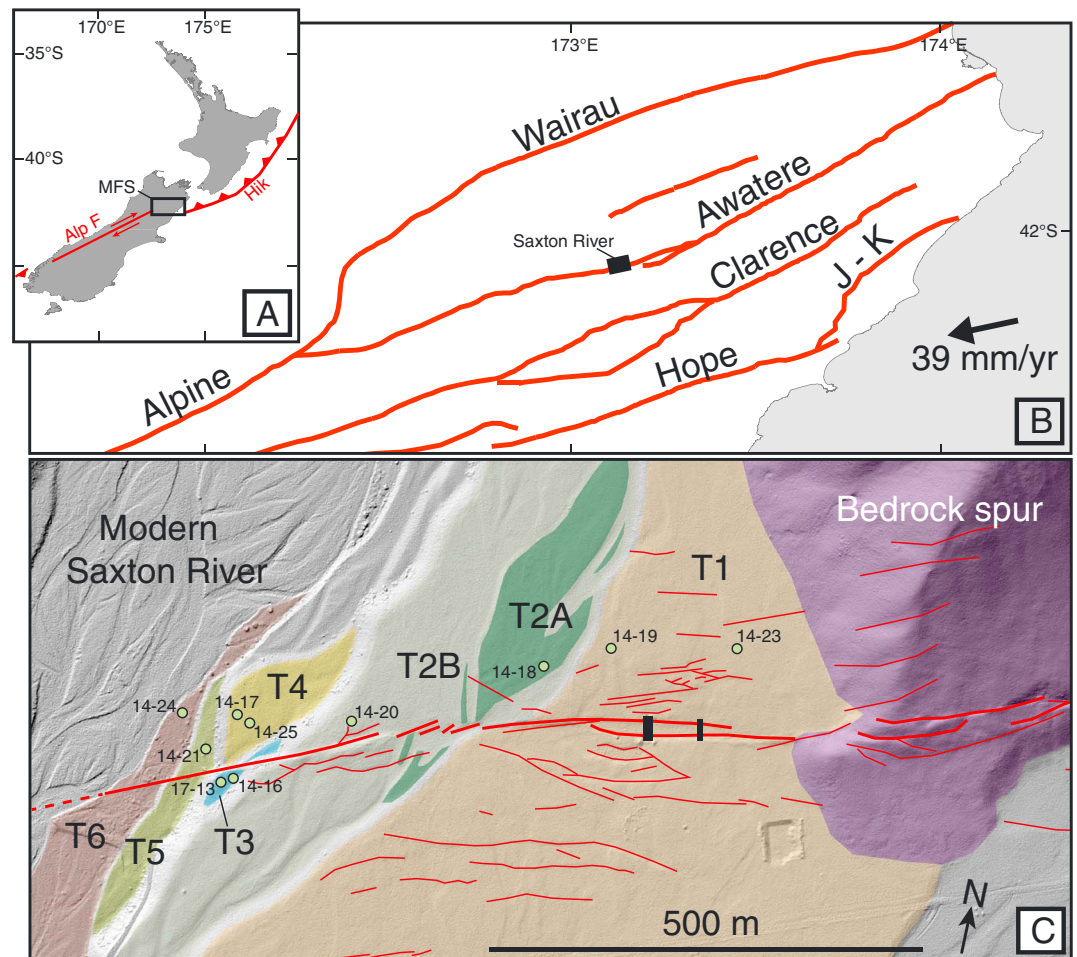


Figure 1. (a) Tectonic map of New Zealand. The MFS is a system of faults that transfer strain between the Alpine fault (Alp F) and Hikurangi subduction zone (Hik). (b) Major strike-slip faults of the MFS (J-K is Jordan-Kekerengu fault). The black arrow indicates NUVEL-1A relative plate motion vector (DeMets et al., 1994). (c) the Saxton River site comprises six terraces and a bedrock promontory, shown by colors on lidar hillshade. The green dots are sample pits, labeled by location number. The black rectangles are paleoseismic trenches by Mason (2004).

S1 in the supporting information) (e.g., Mason et al., 2006). Terrace risers are the scarps between terrace surfaces and are denoted herein by the older tread separated from the younger tread by a forward slash (e.g., T5/T6). Progressive strike slip along the Awatere fault has been recorded by the terrace features and bedrock spur, resulting in a time-transgressive sequence of fault offsets. Using different techniques for measuring and dating the offset features, previous researchers have concluded that the slip rates were either constant (Lensen, 1973; Mason et al., 2006) or variable through time (Knuepfer, 1992; McCalpin, 1996; Gold & Cowgill, 2011).

3. Offset Determinations

To measure the geomorphically expressed displacements recorded at Saxton River, we combined mapping using high-resolution aerial lidar microtopographic data (<http://www.opentopography.org/>) (Dolan & Rhodes, 2016); Figure S1 and Text S2 in the supporting information), with observations made during 2012, 2014, and 2017 field seasons. We identified six offset features that can be unequivocally restored across the fault, and a potential seventh that provides a robust maximum estimate of slip (Figures 2 and S3). These include, from oldest and most-offset, to youngest and least-offset: (1) a bedrock ridge crest and associated T1/bedrock onlap (i.e., terrace inner edge) contact, (2) the potential edge of initial river incision into T1, (3) channel bed forms within the T2 surface, (4) the T1/T2 riser, (5) the T2B/T3 riser, (6) the T3–T4/T5 riser, and

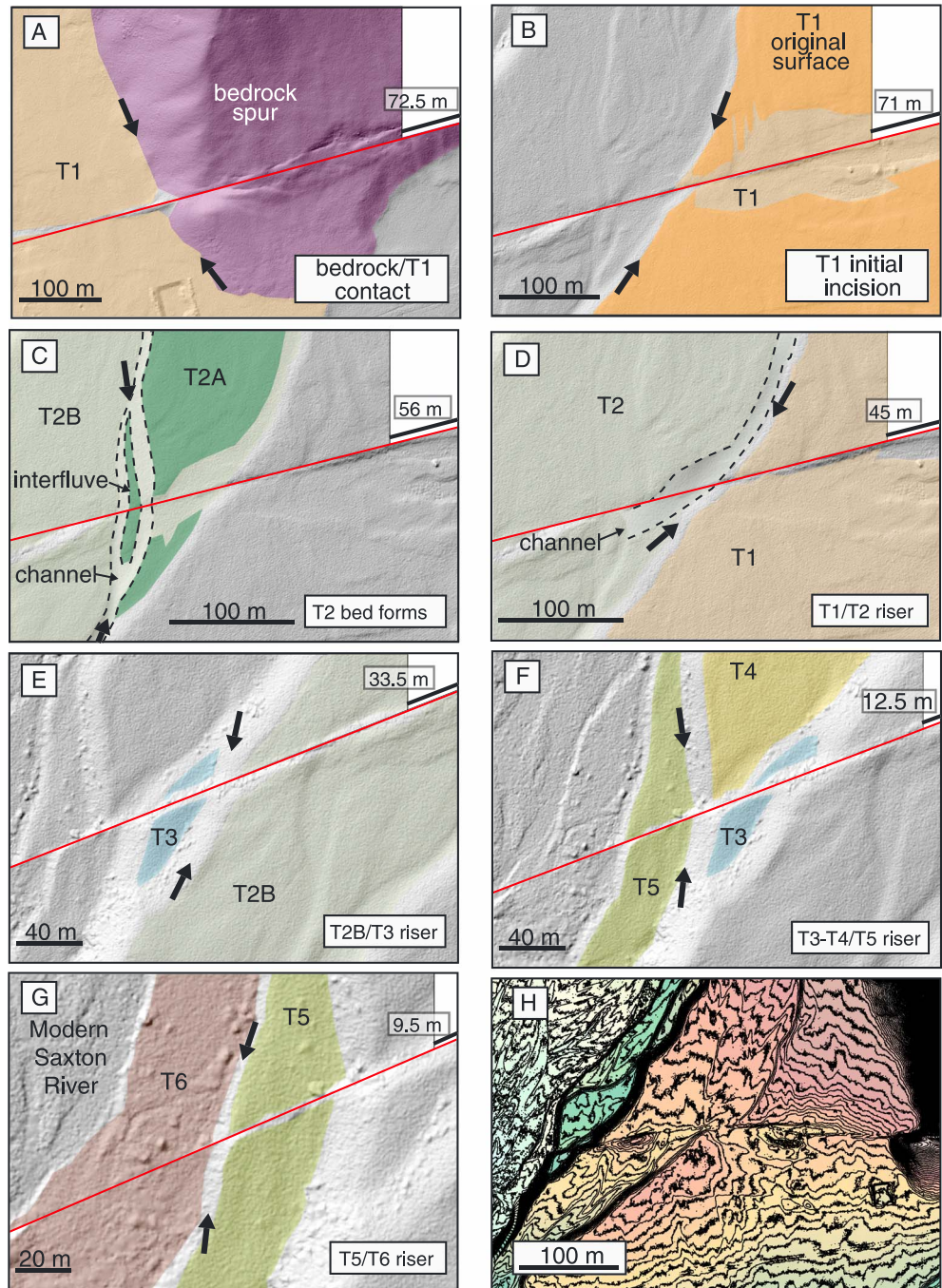


Figure 2. (a–g) Hillshaded lidar maps showing preferred restorations for offset geomorphic features. The arrows show the primary feature(s) restored in each panel: (a) T1/bedrock contact; (b) edge of T1 original (uneroded) surface marks possible edge of initial fluvial incision into T1; (c) remnant bed forms within T2, predating final T1/T2 modification; (d) T1/T2 riser and channel at base of riser, shaped by fluvial erosion during latest stages of T2 occupation; (e) T2B/T3 riser; (f) T3–T4/T5 riser; and (g) T5–T6 riser. (h) 50 cm contour map on DTM colored by elevation.

(7) the T5/T6 riser. Using hillshaded, contoured topography, and other visualizations of a lidar-derived 33 cm per pixel digital terrain model (DTM), we progressively back-slipped one side of each offset feature relative to the other until we determined the maximum and minimum sedimentologically plausible offset values, as well as a preferred value range.

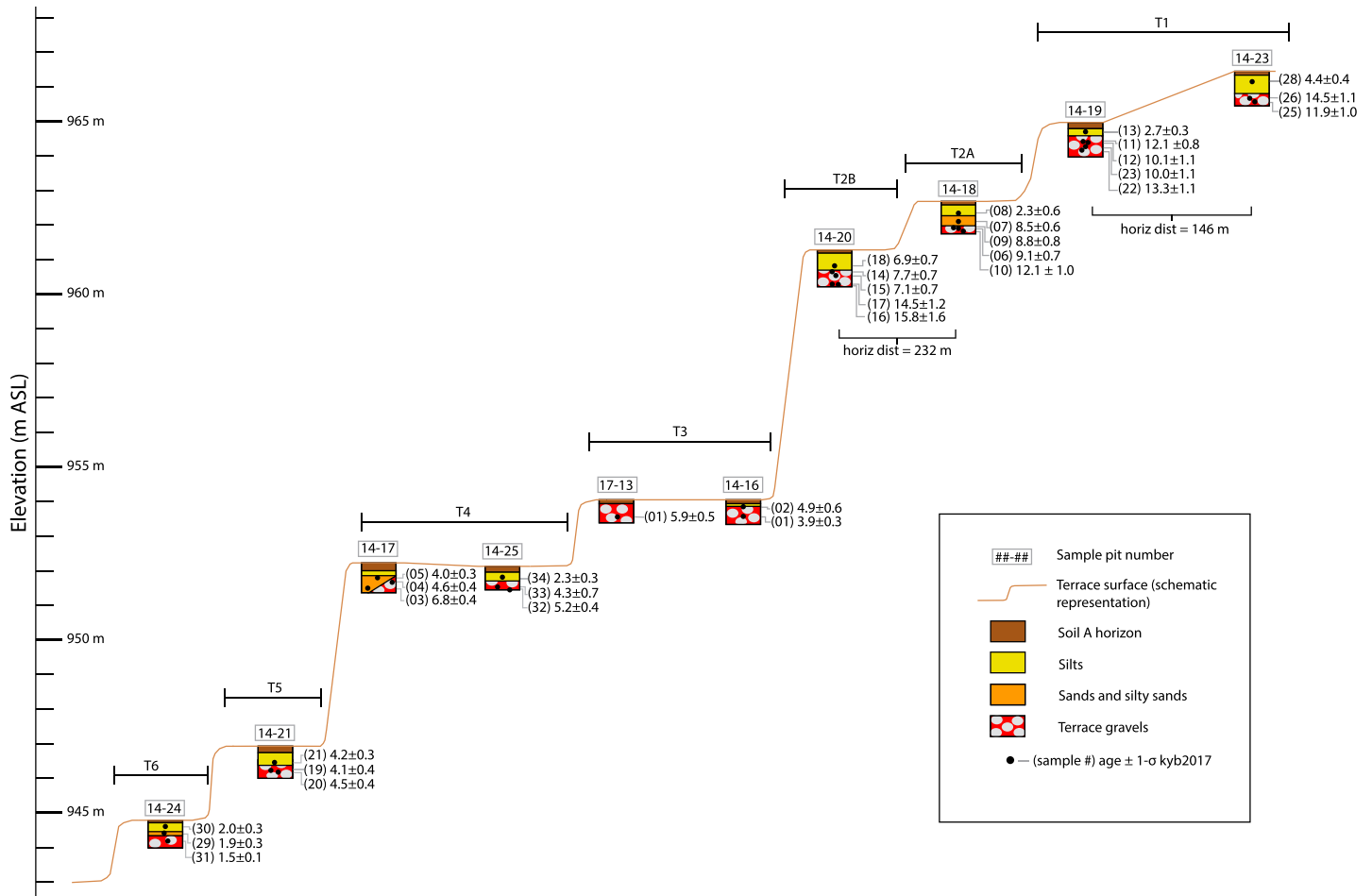


Figure 3. Schematic diagram of IRSL sample pits, labeled by pit number in terraces (T1–T6). The black dots represent IRSL samples and corresponding uncalibrated sample ages within the stratigraphic context of each pit. Elevation in meters above sea level (asl); all horizontal distances arbitrary except where indicated.

Many of the offset features were identified in previous studies (Lensen, 1973; Knuepfer, 1992; McCalpin, 1996; Mason et al., 2006), and generally, our offset measurements are similar to those reported by Mason et al. (2006) (Figure S3). However, our lidar data allowed us to determine several key, previously unrecognized geomorphic relationships. For example, the lidar data reveal subtle bed forms within the T2 surface that suggest that the T2 terrace and T1/T2 riser underwent a complex, multistage geomorphic history (Figure S3). Specifically, an older, higher terrace remnant (T2A) is separated from a younger, lower floodplain (T2B)—an observation that is supported by our age estimate data, described below. Two sets of channels within the broader T2 terrace are offset more than the T1/T2 riser (56 ± 2.0 m and 45 ± 3.0 m, respectively; explained below). Additionally, the cusped geometry of the T1/T2 riser and adjacent channel (Figures 2d and S3) indicate that a late stage of lateral incision cut the riser embankment, and overprinted, but did not completely obliterate, the older channel features in T2. This late stage of T2 erosion may or may not have modified the edge of the original T1 surface north of the fault, which marks initial river incision into the T1 fill terrace, indicating that this is a maximum-possible offset for the T1/T2 riser.

4. Age Determinations

We collected 36 luminescence samples from 10 hand-dug pits in the terraces (Figure 3 and Text S4). The terrace stratigraphy revealed by the pit excavations typically consists of one or more bed load gravel units (pebble–boulder-sized clasts in a silty sand matrix) that are generally capped by silts and soils. The abandonment age of each terrace is represented by the youngest sand or gravel floodplain bed load deposits in each

pit, as these coarse-grained deposits record the final phase of deposition during which the river had the erosive capacity to laterally trim the channel margins. Most terraces at Saxton River are capped by silt deposits (typically ≤ 60 cm thick). These silts were deposited either during the waning stages of floodplain occupation (during which streampower was insufficient to laterally trim the coarse-grained terrace risers), or post-abandonment avulsion events, or as eolian deposits. The silt ages therefore provide a robust minimum age for the sands and gravels in each pit. In some pits, older phases of gravel deposition are recorded beneath the younger bed load gravels. These older deposits, which are in most instances lithologically indistinguishable from the overlying gravel deposits, provide a maximum age for the most recent bed load gravel deposition. Gravel luminescence samples were taken from the sandy matrix.

Thirty four of the IRSL samples were processed according to the newly developed post-IR-IRSL₂₂₅ single K K-feldspar grain procedure (Huntley & Baril, 1997; Rhodes, 2015; Lewis et al., 2017). Age estimates are reported in thousands of years before 2017 (kyb2017). We calculated the terrace tread abandonment ages using a two-step OxCal Bayesian statistical model (further details in Text S4 (Bronk Ramsey, 2001; Rhodes et al., 2003)): First, we undertook a Bayesian model for each pit individually, using the lithostratigraphic observations as input to create sequences of ordered samples within OxCal (step 1), providing us with posterior age estimates for each sample constrained by the results of the other samples in their respective pits. Second, we built a morphostratigraphic sequence age model for the different terraces, incorporating the terrace risers as OxCal boundaries between dating results for each terrace. The age distributions constrained by lithostratigraphic observation in step 1 were input within a phase for each terrace, using only the results from sand or gravel deposited during the latest stage of floodplain occupation. This two-step Bayesian age model approach allows us to make use of all available IRSL data in order to constrain the ages of terrace occupation and deposition, and the ages of the different terrace risers.

Finally, we consider that the samples from an individual bed load gravel or sand deposit represent the age range of that deposit, which we term a “deposit age” (Text S4). In order to estimate this age range we sum all the step 2 posterior age distributions from that deposit. This approach makes no specific assumptions regarding the duration of development of each deposit and provides a conservative measure of the age uncertainty that we use to date each terrace abandonment event.

5. Slip Rate Determinations

The incremental slip rate history of the Awatere fault at Saxton River is determined by matching terrace ages with the geomorphic offsets. Lensen (1964, 1973) suggested that for rivers capable of laterally trimming faulted risers, the riser age is best constrained by the youngest bed load gravels on the lower terrace floodplain. Geomorphic evidence and sedimentological reasoning indicate that this model, referred to as a “lower-terrace reconstruction” (Cowgill, 2007), applies to most of the offset terrace risers at Saxton River (Text S5). Specifically, (1) the coarse, sand, or pebble-boulder grain size of the terrace bed load gravels that we sampled indicates deposition by high-energy flows with high erosive power to trim risers. (2) Right-lateral displacement of a terrace riser on the eastern bank of Saxton River exposes the downstream section of the riser directly to Saxton River streamflow, creating an “exposed corner” susceptible to fluvial erosion, rather than shielding it (e.g., Bull, 1991; McGill & Sieh, 1993). (3) The terrace risers exhibit little evidence of diachroneity (e.g., different slopes north and south of the fault) that might potentially indicate incomplete trimming of the risers during lower terrace floodplain occupation (Cowgill, 2007; Gold et al., 2009).

In contrast to the erosional geomorphic features discussed below, the T1/bedrock contact is a depositional feature that records the onlap of the T1 “fill terrace” floodplain gravels onto the underlying bedrock ridge that formed the valley wall. The 72.5 ± 7.5 m offset of the T1/bedrock contact is therefore dated by the most recent phase of fluvial gravel deposition in the easternmost T1 pit ($12.9 + 1.2/-1.0$ kyb2017). Thus, the average latest Pleistocene-Holocene slip rate of the Awatere fault at Saxton River is $5.6 + 0.4/-0.3$ mm/yr.

T1 terrace abandonment coincided with initial incision into the T1 surface. The edge of the original T1 surface (offset $71 + 2.0/-17$ m; Figure 2b) is best dated by the youngest bed load gravels in the western T1 pit, nearest the T1/T2 riser ($11.3 + 1.4/-1.2$ kyb2017), which provides a robust maximum age for initial T1 incision.

The T2 bed forms are incised into T2A (Figure 2c), indicating that they are younger than the youngest T2A bed load gravels. However, the bed forms are not incised into T2B and are therefore older than the

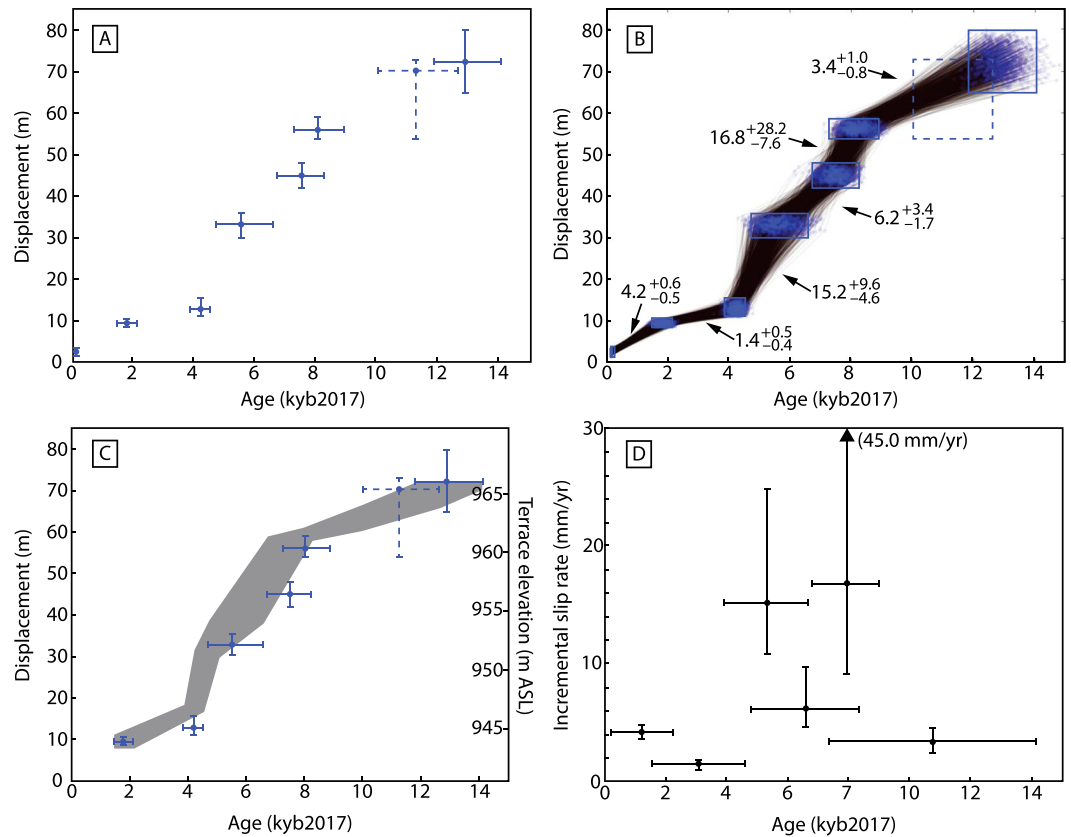


Figure 4. (a) Displacements and ages of offset features. The error bars show 95% uncertainty limits. (b) Monte Carlo sampling of displacements and ages yields incremental slip rates (mm/yr \pm 1-sigma uncertainties) for each interval. (c) Terrace tread elevation versus tread age (gray field) superimposed on incremental fault slip history. Note that Saxton River incision rate generally tracks incremental fault slip rate, suggesting that incision may be controlled by local base level changes related to vertical tectonic motions. (d) Incremental slip rates versus feature age. In Figures 4a and 4c, the potential edge of initial incision into T1 is shown as dashed line.

youngest gravels in T2B. We therefore use the boundary age between the T2A and T2B surfaces (which encompasses the T2A and T2B terrace ages, and all ages in between), yielding $56 \pm 3.0/-2.0$ m of slip since 8.1 ± 0.8 kyb2017.

The T1/T2 riser is the youngest, least-offset feature associated with T2 (Figure 2d). The channel system that was responsible for final shaping of the T1/T2 riser crosscuts all other features preserved in T2 and is incised into the T2B surface. The age of T2B therefore represents a likely close maximum age ($7.6 \pm 0.7/-0.8$ kyb2017) for the 45 ± 3.0 m T1/T2 riser offset.

Both the T3–T4/T5 and T2B/T3 risers are dated by their respective adjacent lower terrace treads (Figure S3 and Text S5). The $12.5 \pm 3.0/-1.5$ m T3–T4/T5 riser offset is dated by T5 floodplain abandonment ($4.3 \pm 0.3/-0.4$ kyb2017), and the $33.5 \pm 2.5/-3.5$ m T2B/T3 riser offset is dated by T3 floodplain abandonment at 5.2 ± 0.5 kyb2017.

The 9.5 ± 1.0 m of offset recorded by the T5/T6 riser is best dated by the gravel age of the T6 terrace tread (1.8 ± 0.3 kyb2017). This offset and age are supported by the Mason (2004) paleo-earthquake record from their T1 trench (Figure S6), as well as by the smallest (~ 2.5 m) geomorphic offsets observed just east of Saxton River (Mason, 2004; Zinke et al., 2016). Specifically, the most recent surface-rupturing earthquake (MRE) at Saxton River occurred <300 calendar year B.P. (Mason, 2004). This event (inferred to be the 16 October 1848 M 7.4–7.5 Marlborough earthquake (Grapes et al., 1998; Mason, 2004)) was the most recent of an apparent four-event cluster of events that likely occurred during the past c.1 kyr (i.e., since T6 was abandoned c.1.8 ka) (Mason, 2004). If each of these four events had ~ 2.5 m of slip, the resulting ~ 10 m of slip closely matches the 9.5 ± 1.0 m offset we determine for the T5/T6 riser. Moreover, the

paleo-earthquake age data appear to support a preceding period of slow slip, with only two additional surface ruptures documented between c.1 ka and 4 ka (Mason, 2004). This supports our lower-terrace reconstruction and use of the $4.3 + 0.3/-0.4$ kyr2017 abandonment age for T5 to date the $12.5 + 3.0/-1.5$ m T3–T4/T5 riser offset. We include the age and displacement of the MRE in our final analysis of incremental slip rates.

Incremental slip rates were calculated using a Monte Carlo sampling technique (Text S7). Our method is similar to that of Gold and Cowgill (2011) in that it discards values that result in negative (i.e., left-lateral) slip rates; however, our sampling scheme draws random displacement and age values according to the probability density functions of each respective measurement, allowing for propagation of uncertainties. The resulting incremental slip rates (Figure 4 and Table S8 in the supporting information) between geomorphic features are $3.4 + 1.0/-0.8$ mm/yr (T1/bedrock contact to T2 bed forms), $16.8 + 28.2/-7.6$ mm/yr (T2 bed forms to T1/T2 riser), $6.2 + 3.4/-1.7$ mm/yr (T1/T2 riser to T2B/T3 riser), $15.2 + 9.6/-4.6$ mm/yr (T2B/T3 riser to T3–T4/T5 riser), $1.4 + 0.5/-0.4$ mm/yr (T3–T4/T5 riser to T5/T6 riser), and $4.2 + 0.6/-0.5$ mm/yr (T5/T6 riser to MRE).

6. Discussion and Conclusions

The new age and displacement data described above demonstrate that incremental slip rates of the Awatere fault at Saxton River varied by a factor of ~ 12 , over tens of meters of slip and millennial timescales during Holocene and latest Pleistocene time (Figure 4). During latest Pleistocene and early Holocene time (~ 12 –8 ka), the fault exhibited a relatively slow slip rate of ~ 3 mm/yr. This was followed by a period of exceptionally rapid slip rate (three separate rates that range from ~ 6 to 17 mm/yr), involving ~ 45 m of slip between ~ 4 –8 ka. Subsequently, since ~ 4 ka the fault has been slipping at a much slower slip rate of ~ 3 mm/yr, encompassing a period of extremely slow (~ 1.4 mm/yr) slip rate between ~ 1.8 and 4.3 ka.

Importantly, all of these slip rate data were documented at the same site, providing a robust record of fault behavior that is not complicated by potentially temporally different fault behavior at widely separated sites along strike. The extreme slip rate variability observed at Saxton River raises important issues about the mechanics of fault behavior and the use of geologic slip rates in seismic hazard analysis and the search for strain transients.

Specifically, these extreme rate changes suggest the possibility that either the strength of the fault is varying through time and/or that the rate of elastic strain accumulation has changed with time. For example, it has been proposed that variations in slip rate could be caused by alternating periods of fault strengthening and weakening, controlled by either temporal changes to the fault zone rocks themselves (e.g., Chéry & Vernant, 2006; Dolan et al., 2007; Oskin et al., 2008; Dolan et al., 2016), or by addition or removal of gravitational loads (e.g., Hetzel & Hampel, 2005; Luttrell & Sandwell, 2010). Alternatively, others have suggested that variations in slip rate could be controlled by external factors, such as regional kinematic fault interactions (Dolan et al., 2007), or true temporal changes in relative plate motion rate (e.g., Anderson, 1975; Romanowicz, 1993; Pollitz et al., 1998; Dolan et al., 2016; Meade & Loveless, 2017). Whatever the causes of the variable slip rate behavior at Saxton River, these data add to a growing list of examples from other faults that exhibit temporally variable slip rates (e.g., Wallace, 1987; Friedrich et al., 2003; Weldon et al., 2004; Dolan et al., 2007, 2016; Sieh et al., 2008; Gold & Cowgill, 2011; Goldfinger et al., 2013; Ninis et al., 2013; Onderdonk et al., 2015).

The possibility that such variations in rate could be more common than generally thought, perhaps masked by the dearth of well-constrained incremental slip rate records, raises concern about comparisons of geologic and geodetic rates in the search for strain transients: When comparing such data sets, what is the “correct” slip rate to use? In the case of Saxton River, if the rate of elastic strain accumulation on the Awatere fault has remained constant through latest Pleistocene–Holocene time at ~ 5.5 mm/yr (based on the ~ 13 ka average slip rate we determined), use of the very slow (~ 1.4 mm/yr) slip rate averaged between 1.8 and 3.3 ka might be interpreted as an example in which the rate of elastic strain accumulation far exceeds the “long-term” geologic slip rate. In contrast, if we had happened upon Saxton River ~ 4 kyr ago, at the end of the mid-Holocene period of extremely fast slip, especially at the end of either of the exceptionally fast periods ~ 8 ka and 5–6 ka (~ 17 and ~ 15 mm/yr), comparison with the geodetic data might have suggested that the fault was storing elastic strain energy much more slowly than the geologic slip rate.

Such extreme variations in rate suggest the alternative possibility that the rate of elastic strain accumulation along the Awatere fault may not have remained constant through time. While it is impossible to directly document any potential mid-Holocene changes in elastic strain accumulation rate, an acceleration in strain accumulation could help to explain the extreme variation between the late-Holocene period of slow slip and the preceding period of very rapid slip. In another possible example of such behavior, Dolan et al. (2016) noted that in the San Andreas Fault (SAF) Wrightwood record (Weldon et al., 2004), within each of the three-to five-earthquake-long periods of alternating slow (~15 mm/yr) and fast (~89 mm/yr) slip rate at that site, the rate of elastic strain release yielded a relatively continuous slip rate within each period. This suggests that the SAF may be “keeping up” with a variable elastic strain accumulation rate that remained relatively constant over tens of meters of slip and multiple earthquakes within each supercycle (Dolan et al., 2016). To provide context for the degree to which Saxton River slip rates vary temporally, the variation in rate at Wrightwood between three to five earthquake-long fast and slow periods is a factor of ~6 (~15 versus ~90 mm/yr). Assuming, as discussed above, that the average slip per event at Saxton River was ~2.5 m, the millennial-scale slip rate variations there likely also spanned three to five or more earthquakes, similar to the number of events in each fast or slow period at Wrightwood. But the resulting factor of ~12 rate variation on the Awatere fault is even more extreme than at Wrightwood. These observations demonstrate the need for caution in comparing geodetic and geologic slip rates.

The slip rate variations revealed by the Saxton River data also raise important concerns about the use of geologic slip rates in seismic hazard analysis. Geologic slip rates are a basic input for most probabilistic seismic hazard models (e.g., UCERF3 (Field et al., 2014, 2015, 2017)). In situations such as Saxton River, however, the resulting probabilities of earthquake occurrence will covary with the different incremental slip rates through time. For example, if we only used a slip rate averaged over the late-Holocene slow period, the resulting seismic hazard would be relatively low. Conversely, if we happened to measure the slip rate at the end of the mid-Holocene fast period, the resulting earthquake probabilities would be approximately an order of magnitude higher. It might therefore be tempting to simply use longer-term slip rates averaged over many tens to hundreds of kiloyears, with the expectation that rate variations may average out over these time-scales. However, slip rates have been shown to vary in some systems over longer timespans due to fault evolution, changes in relative plate boundary motions, or other causes (e.g., Wallace, 1987; Marco et al., 1996; Friedrich et al., 2003; Bergen et al., 2017). Resolution of this problematic issue will require the addition of many more incremental slip rate records, similar to the one we document at Saxton River, for many more faults in different tectonic settings and over a wide range of timescales. Comprehensive incremental slip rate records from all major faults in a fault system are required to understand system-level behavior through time, which will in turn facilitate a system-level search for causes, as well as the predictability of slip rate variability.

Acknowledgments

This research was funded by U.S. National Science Foundation grants EAR-1321914 (Dolan) and EAR-1321912 (Rhodes) and by GNS Science. Our manuscript benefitted from reviews by George Hilley and an anonymous reviewer. We thank Alex Hatem, Rob Langridge, and Charlie Sammis for helpful discussions and Jess Grenader, Juliet Olsen, Mike Say, and Nathan Brown for field and technical assistance. Special thanks to Jim and Tracy Ward, and Steve and Mary Satterthwaite for their kind permission to work on their land, and Neil Fowke (N.Z. Department of Conservation) for assistance with permitting. Data used in this study can be found in the supporting information (S1–S8).

References

- Anderson, D. L. (1975). Accelerated plate tectonics. *Science*, *187*(4181), 1077–1079.
- Bergen, K. J., Shaw, J. H., Leon, L. A., Dolan, J. F., Pratt, T. L., Ponti, D. J., ... Owen, L. A. (2017). Accelerating slip rates on the Puente Hills blind thrust fault system beneath metropolitan Los Angeles, California, USA. *Geology*, *45*(3), 227–230. <https://doi.org/10.1130/G38520.1>
- Bronk Ramsey, C. (2001). Development of the radiocarbon program OxCal. *Radiocarbon*, *43*(2A), 355–363. <https://doi.org/10.1017/S0033822200038212>
- Bull, W. B. (1991). *Geomorphic Responses to Climate Change*. Oxford: Oxford University Press.
- Bull, W. B., & Knuepfer, P. L. K. (1987). Adjustments by the Charwell River, New Zealand, to uplift and climatic changes. *Geomorphology*, *1*(1), 15–32. [https://doi.org/10.1016/0169-555X\(87\)90004-3](https://doi.org/10.1016/0169-555X(87)90004-3)
- Chéry, J., & Vernant, P. (2006). Lithospheric elasticity promotes episodic fault activity. *Earth and Planetary Science Letters*, *243*(1–2), 211–217. <https://doi.org/10.1016/j.epsl.2005.12.014>
- Cowgill, E. (2007). Impact of riser reconstructions on estimation of secular variation in rates of strike-slip faulting: Revisiting the Cherven River site along the Altyn Tagh fault, NW China. *Earth and Planetary Science Letters*, *254*(3–4), 239–255. <https://doi.org/10.1016/j.epsl.2006.09.015>
- DeMets, C., Gordon, R. G., Argus, D. F., & Stein, S. (1994). Effects of recent revisions to the geomagnetic reversal time scale on estimates of current plate motions. *Geophys. Res. Lett.*, *21*, 2191–2194. <https://doi.org/10.1029/94GL02118>
- Dolan, J. F., Bowman, D. D., & Sammis, C. G. (2007). Long-range and long-term fault interactions in Southern California. *Geology*, *35*(9), 855–858. <https://doi.org/10.1130/G23789A.1>
- Dolan, J. F., McAuliffe, L. J., Rhodes, E. J., McGill, S. F., & Zinke, R. (2016). Extreme multi-millennial slip rate variations on the Garlock fault, California: Strain super-cycles, potentially time-variable fault strength, and implications for system-level earthquake occurrence. *Earth and Planetary Science Letters*, *446*, 123–136. <https://doi.org/10.1016/j.epsl.2016.04.011>
- Dolan, J. F., & Rhodes, E. J. (2016). *Marlborough Fault System, South Island, New Zealand*, National Center for Airborne Laser Mapping. Retrieved from <http://opentopography.org>, <https://doi.org/10.5069/G9G44N75>

- Field, E. H., Arrowsmith, J. R., Biasi, G. P., Bird, P., Dawson, T. E., Felzer, K. R., ... Zeng, Y. (2014). Uniform California earthquake rupture forecast, version 3 (UCERF 3): The time-independent model. *Bulletin of the Seismological Society of America*, *104*(3), 1122–1180. <https://doi.org/10.1785/0120130164>
- Field, E. H., Biasi, G. P., Bird, P., Dawson, T. E., Felzer, K. R., Jackson, D. D., ... Zeng, Y. (2015). Long-term time-dependent probabilities for the third uniform California earthquake rupture forecast (UCERF3). *Bulletin of the Seismological Society of America*, *105*(2A), 511–543. <https://doi.org/10.1785/0120140093>
- Field, E. H., Jordan, T. H., Page, M. T., Milner, K. R., Shaw, B. E., Dawson, T. E., ... Thatcher, W. R. (2017). A synoptic view of the third uniform California earthquake rupture forecast (UCERF3). *Seismological Research Letters*, *88*(5), 1259–1267. <https://doi.org/10.1785/0220170045>
- Friedrich, A. M., Wernicke, B. P., Niemi, N. A., Bennett, R. A., & Davis, J. L. (2003). Comparison of geodetic and geologic data from the Wasatch region, Utah, and implications for the spectral character of Earth deformation at periods of 10 to 10 million years. *Journal of Geophysical Research*, *108*(B4), 2199. <https://doi.org/10.1029/2001JB000682>
- Gold, R. D., & Cowgill, E. (2011). Deriving fault-slip histories to test for secular variation in slip, with examples from the Kunlun and Awatere faults. *Earth and Planetary Science Letters*, *301*(1–2), 52–64. <https://doi.org/10.1016/j.epsl.2010.10.011>
- Gold, R. D., Cowgill, E., Arrowsmith, J. R., Gosse, J., Chen, X., & Wang, X.-F. (2009). Riser diachroneity, lateral erosion, and uncertainty in rates of strike-slip faulting: A case study from Tuzidun along the Altyn Tagh fault, NW China. *Journal of Geophysical Research*, *114*, B04401. <https://doi.org/10.1029/2008JB005913>
- Goldfinger, C., Ikeda, Y., Yeats, R. S., & Ren, J. (2013). Superquakes and supercycles. *Seismological Research Letters*, *84*(1), 24–32. <https://doi.org/10.1785/0220110135>
- Grapes, R., Little, T., & Downes, G. (1998). Rupturing of the Awatere fault during the 1848 October 16 Marlborough earthquake, New Zealand: Historical and present day evidence. *New Zealand Journal of Geology and Geophysics*, *41*(4), 387–399. <https://doi.org/10.1080/00288306.1998.9514818>
- Hetzl, R., & Hampel, A. (2005). Slip rate variations on normal faults during glacial–interglacial changes in surface loads. *Nature*, *435*(7038), 81–84. <https://doi.org/10.1038/nature03562>
- Huntley, D. J., & Baril, M. (1997). The K content of the K-feldspar being measuring in optical dating or in thermoluminescence dating. *Ancient TL*, *15*, 11–13.
- Knuepfer, P. L. K. (1992). Temporal variations in latest quaternary slip across the Australian-Pacific plate boundary, north-eastern South Island, New Zealand. *Tectonics*, *11*(3), 449–464. <https://doi.org/10.1029/91TC02890>
- Lensen, G. J. (1964). The general case of progressive fault displacement of flights of degradational terraces. *New Zealand Journal of Geology and Geophysics*, *7*(4), 871–876. <https://doi.org/10.1080/00288306.1964.10428135>
- Lensen, G. J. (1973). Guidebook for excursion A10, in International Union for Quaternary Research Congress: Christchurch, New Zealand, 9th Congress, Field Trip Guide, 76 p.
- Lewis, C. J., Sancho, C., McDonald, E. V., Peña-Monné, J. L., Puelo, E. L., Rhodes, E. J., ... Soto, R. (2017). Post-tectonic landscape evolution in NE Iberia using a staircase of terraces: Combined effects of uplift and climate. *Geomorphology*, *292*, 85–103. <https://doi.org/10.1016/j.geomorph.2017.04.037>
- Luttrell, K., & Sandwell, D. (2010). Ocean loading effects on stress at near shore plate boundary fault systems. *Journal of Geophysical Research*, *115*, B08411. <https://doi.org/10.1029/2009JB006541>
- Marco, S., Stein, M., & Agnon, A. (1996). Long-term earthquake clustering: A 50,000-year paleoseismic record in the Dead Sea Graben. *Journal of Geophysical Research*, *101*(B3), 6179–6191. <https://doi.org/10.1029/95JB01587>
- Mason, D. P. M. (2004). Neotectonics and paleoseismicity of a major junction between two strands of the Awatere Fault, South Island, New Zealand [M.S. thesis]: Wellington, New Zealand, Victoria University of Wellington, 173 p.
- Mason, D. P. M., Little, T. A., & Van Dissen, R. J. (2006). Rates of active faulting during late quaternary fluvial terrace formation at Saxton River, Awatere fault, New Zealand. *Geological Society of America Bulletin*, *118*(11–12), 1431–1446. <https://doi.org/10.1130/B25961.1>
- McCalpin, J. P. (1996). Tectonic geomorphology and Holocene paleoseismicity of the Molesworth section of the Awatere fault, South Island, New Zealand. *New Zealand Journal of Geology and Geophysics*, *39*(1), 33–50. <https://doi.org/10.1080/00288306.1996.9514693>
- McGill, S., & Sieh, K. (1993). Holocene slip rate of the central Garlock fault in southeastern Searles Valley, California. *Journal of Geophysical Research*, *98*(B8), 14,217–14,231. <https://doi.org/10.1029/93JB00442>
- Meade, B. J., & Loveless, J. P. (2017). Block motion changes in Japan triggered by the 2011 Great Tohoku Earthquake. *Geochemistry, Geophysics, Geosystems*, *18*, 2459–2466. <https://doi.org/10.1002/2017GC006983>
- Ninis, D., Little, T. A., Van Dissen, R. J., Litchfield, N. J., Smith, E. G. C., Wang, N., ... Henderson, C. M. (2013). Slip rate on the wellington fault, New Zealand, during the late quaternary: Evidence for variable slip during the Holocene. *Bulletin of the Seismological Society of America*, *103*(1), 559–579. <https://doi.org/10.1785/0120120162>
- Onderdonk, N. W., McGill, S. F., & Rockwell, T. K. (2015). Short-term variations in slip rate and size of prehistoric earthquakes during the past 2000 years on the northern San Jacinto fault zone, a major plate-boundary structure in southern California. *Lithosphere*, *7*(3), 211–234. <https://doi.org/10.1130/L393.1>
- Oskin, M., Perg, L., Shelef, E., Strane, M., Gurney, E., Singer, B., & Zhang, X. (2008). Elevated shear zone loading rate during an earthquake cluster in eastern California. *Geology*, *36*(6), 507–510. <https://doi.org/10.1130/G24814A.1>
- Pollitz, F. F., Bürgmann, R., & Romanowicz, B. (1998). Viscosity of oceanic asthenosphere inferred from remote triggering of earthquakes. *Science*, *280*(5367), 1245–1249. <https://doi.org/10.1126/science.280.5367.1245>
- Rhodes, E. J. (2015). Dating sediments using potassium feldspar single-grain IRSL: Initial methodological considerations. *Quaternary International*, *362*, 14–22. <https://doi.org/10.1016/j.quaint.2014.12.012>
- Rhodes, E. J., Bronk-Ramsey, C., Outram, Z., Batt, C., Willis, L., Dockrill, S., & Bond, J. (2003). Bayesian methods applied to the interpretation of multiple OSL dates: High precision sediment age estimates from old Scatness Broch excavations, Shetland isles. *Quaternary Science Reviews*, *362*, 14–22. <https://doi.org/10.1016/j.quaint.2014.12.012>
- Romanowicz, B. (1993). Spatiotemporal patterns in the energy release of great earthquakes. *Science*, *260*(5116), 1923–1926. <https://doi.org/10.1126/science.260.5116.1923>
- Sieh, K., Natawidjaja, D. H., Meltzner, A. J., Shen, C.-C., Cheng, H., Li, K.-S., ... Edwards, R. L. (2008). Earthquake Supercycles inferred from sea-level changes recorded in the corals of West Sumatra. *Science*, *322*(5908), 1674–1678. <https://doi.org/10.1126/science.1163589>
- Tapponnier, P., & Molnar, P. (1976). Slip-line field theory and large-scale continental tectonics. *Nature*, *264*(5584), 319–324. <https://doi.org/10.1038/264319a0>
- Wallace, L. M., Barnes, P., Beavan, J., Van Dissen, R., Litchfield, N., Mountjoy, J., ... Pondard, N. (2012). The kinematics of a transition from subduction to strike-slip: An example from the central New Zealand plate boundary. *Journal of Geophysical Research*, *117*, B02405. <https://doi.org/10.1029/2011JB008640>

- Wallace, R. E. (1987). Grouping and migration of surface faulting and variations in slip rates on fault in the Great Basin province. *Bulletin of the Seismological Society of America*, 77(3), 868–876. <https://doi.org/10.1029/2008RG000260>
- Weldon, R., Scharer, K., Fumal, T., & Biasi, G. (2004). Wrightwood and the earthquake cycle: What a long recurrence record tells us about how faults work. *GSA Today*, 14(9), 4. <https://doi.org/10.1130/1052-5173>
- Zinke, R., Dolan, J. F., Hatem, A. E., Van Dissen, R. J., Langridge, R., Grenader, J., ... Nicol, A. (2016). Measuring slip in paleoearthquakes using high-resolution aerial lidar data: Combined analysis of the Wairau, Awatere, Clarence, and Hope faults, South Island, New Zealand: EOS transactions. In Proceedings of the Fall 2016 Annual Meeting, abstract T41B-2924.